54 Study on Blade Wake Interaction Using Grid Refinement Method

by
Choongmo Yang and Jehyun Baek
Department of Mechanical Engineering, POSTECH

ABSTRACT

As a step to develop an accurate solution technique, grid-refined multi-block system in parallel computing was used to solve two-dimensional unsteady Navier-Stokes equations with Baldwin-Lomax turbulence modeling. Flowfields around NACA0012 in several conditions were solved to show effectiveness of the method by comparing several aerodynamic coefficients with experimental data. In the first part, the solver was validated with steady/unsteady test cases to compare the results with experimental data. Flowfields around a NACA0012 airfoil with pitching and/or plunging motions were analyzed by solving two-dimensional unsteady compressible Navier-Stokes equations. An unsteady flowfield of the oscillatory airfoil was solved and compared with experimental data. Grid was refined near airfoil and the wake region following the shed vortex trace to reduce the numerical dissipation and multi-block grids with Zonal boundary were used for efficient calculation using parallel computing. In the second part, flow interactions between wake and airfoil were solved. The shed vortex induced from the oscillating airfoil was applied as inflow condition of the following airfoil using periodic boundary conditions, which is a simplified two-dimensional model of a helicopter rotor blade at the mid-span section. The induced wake of the pitching airfoil, which was affected by the following airfoil, was used with various grid systems to show that refined grid is effective in reducing the numerical dissipation.

1. Introduction

Blade-Wake Interaction (BWI) was introduced more than 20 years ago, and BWI noise was specifically identified by Brook in 1988. Even there are several ways of dividing helicopter noise, if we focus on the spectrum analysis, helicopter was said to have 4 kinds of noise mechanism as shown in figure 1[1].

One is discrete loading noise due to steady and azimuthally dependent blade loading, which dominates the lower harmonics of the blade passage frequency. Next is discrete impulsive noise, or Blade-Vortex Interaction (BVI) noise which is already well known to dominate a large number of harmonics. Broadband noise of Blade-Wake Interaction (BWI) noise is dominant at somewhat higher frequencies because of blade interaction with turbulence in and about the general rotor wake. The last one is broadband self-noise due to blade interaction with boundary layer and near-wake turbulence, which controls the high-frequency part of spectra.

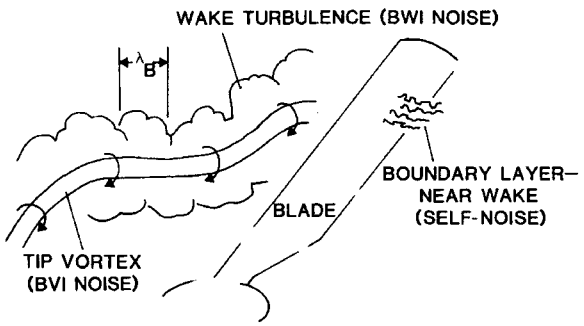

Figure 1. Diagram of noise sources in helicopter rotor

The relative significance of each of these mechanisms is dependent on rotor operating conditions. BVI is, as already known, dominant during decent flight. Blade-Wake Interaction (BWI) is known to be significant in level or climb flight, which is important to human sensitivity[1]. At high climb angles, BWI is reduced and self-noise from blade boundary-layer turbulence becomes the most prominent.

In this paper, BWI was simplified into 2D interaction model. Figure 2 shows the diagram of interaction between shed vortex from oscillating airfoil and following airfoil. This can be figured out to compose one repeated computational domain, and the computational domain can be altered to include one whole blade with fore and rear flow region. To simulate the hovering flight or low-speed forward flight of helicopter rotor, periodic condition can be applied to inflow and outflow boundary conditions.

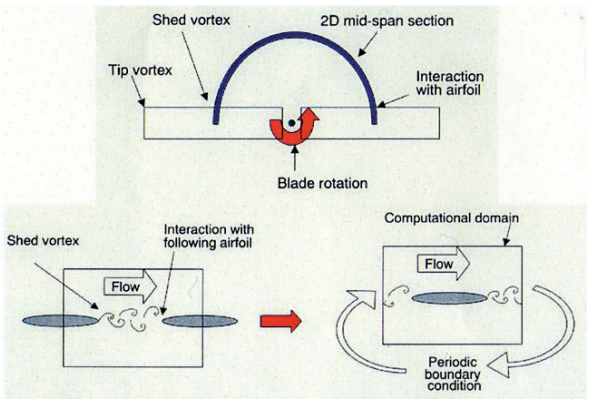

Figure 2. Diagram of interaction between vortex and airfoil

In solving the wake or vortex flow with computational fluid dynamics method, numerical dissipation is one of the important barriers for accurate solution. Up to now many researchers have been trying to overcome these difficulties, specially linked to vortex capturing CFD methods.

Highly accurate schemes allow one to diminish the numerical dissipation but they increase the required CPU time per cell and require extended boundary conditions. Another approach is to use local Eulerian/Lagrangian coupling method but stability and conservation problems may arise. An alternative is to use mesh adaptation using overset grid or refined grid.

For two-dimensional airfoil problem with wake, two grid systems can be easily used for refinement, which is shown in figure 3. C-type grid system (figure 3(a)) is good for grid reduction and attraction to the surface, and also good to capture the wake. But in order to calculate re-entered wake like helicopter rotor, H-type grid (figure 3(b)) will be better for periodic boundary condition and fine grid following the wake.

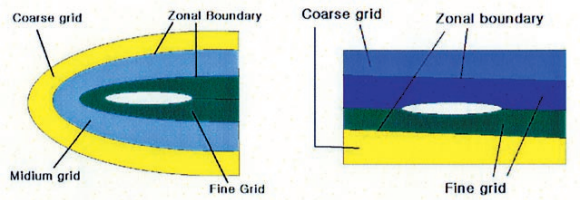

(a) C-type (b) H-type

Figure 3. Diagram of multi-block grid system

In this research, as a step to develop the accurate solution technique, grid-refined multi-block system was used to solve two-dimensional unsteady Navier-Stokes equations in parallel computing with Baldwin-Lomax turbulence modeling. Flowfields around NACA0012 in several conditions were solved to show effectiveness of the method by comparing several aerodynamic coefficients with experimental data.

2. Numerical Method

The governing equations of two-dimensional compressible Navier-Stokes can be written in generalized coordinate system as the followings:

$$\frac{1}{J}\frac{\partial Q}{\partial t}+\frac{\partial(\hat{F}-\hat{F}_v)}{\partial\xi}+\frac{\partial(G-G_v)}{\partial\eta}=0$$

where

$$Q=[\rho,\rho u,\rho v,e]^T$$

$$F=\left[\rho u,\rho u^2+p,\rho uv,u(e+p)\right]^T,$$

$$G=\left[\rho v,\rho uv,\rho v^2+p,v(e+p)\right]^T,$$

$$F_v=\left[0,\tau_{xx},\tau_{xy},u\tau_{xx}+v\tau_{xy}-\dot{q}_x\right]^T,$$

$$G_v=\left[0,\tau_{yx},\tau_{yy},u\tau_{yx}+v\tau_{yy}-\dot{q}_y\right]^T$$

$$\hat{F}=(\xi_xF+\xi_yG)/J,\quad \hat{F}_v=(\xi_xF_v+\xi_yG_v)/J$$

$$\hat{G}=(\eta_xF+\eta_yG)/J,\quad \hat{G}_v=(\eta_xF_v+\eta_yG_v)/J$$

$$J=\frac{\partial(\xi,\eta)}{\partial(x,y)}=\xi_x\eta_y-\xi_y\eta_x=\left[x_\xi y_\eta-x_\eta y_\xi\right]^{-1}$$

In the above equations, ρ is the gas density, u, v the Cartesian velocity components in x, y directions, e is the total energy per unit volume. The pressure p is obtained by the perfect gas equation by

$$p=(\gamma-1)\left[e-\frac{1}{2}\rho(u^2+v^2)\right]$$

where γ is the ratio of specific heats, usually as γ =1.4 for air.

The components of stress tensor derived with the assumption of linear stress-strain relation and Stokes' hypothesis for bulk viscosity are

$$\tau_{xx}=\frac{M_\infty\mu}{\mathrm{Re}_\infty}\frac{2}{3}\left(2u_x-v_y\right),$$

$$\tau_{xx}=\frac{M_\infty\mu}{\mathrm{Re}_\infty}\frac{2}{3}\left(2v_y-u_x\right),$$

$$\tau_{xy}=\tau_{yx}=\frac{M_\infty\mu}{\mathrm{Re}_\infty}\left(u_y+v_x\right)$$

The elements of heat flux vector are expressed by the Fourier law of heat conduction as

$$\dot{q}_x=-\frac{M_\infty\kappa}{\mathrm{Re}_\infty}\frac{\partial T}{\partial x},\quad \dot{q}_y=-\frac{M_\infty\kappa}{\mathrm{Re}_\infty}\frac{\partial T}{\partial y}$$

where T is the temperature and κ is the thermal conductivity.

The inviscid flux vectors are discretized using Roe's flux difference splitting (FDS) method[2]. The flux difference across a cell interface is divided into components associated with each characteristic wave with third order accuracy using TVD scheme[3]. Roe's approximate Riemann solver does not satisfy the entropy condition and thus permits physically inadmissible expansion shock. To remedy this problem, entropy correction is applied

For time integration, Euler Backward Implicit Time Integration was used with 2nd order accuracy using 3 point Euler implicit method.

As a solution algorithm, Upwind Line Gauss-Seidal Relaxation method was used. To simulate viscous turbulent flow, Baldwin-Lomax Algebraic turbulence modeling was used.

3. Results and Discussion

3.1 Validation

Test case for steady flow around RAE2822 airfoil has Mach number equal to 0.73, Reynolds number equal to 6.5×10^6 at the angle of attack, α equal to 2.79 °.

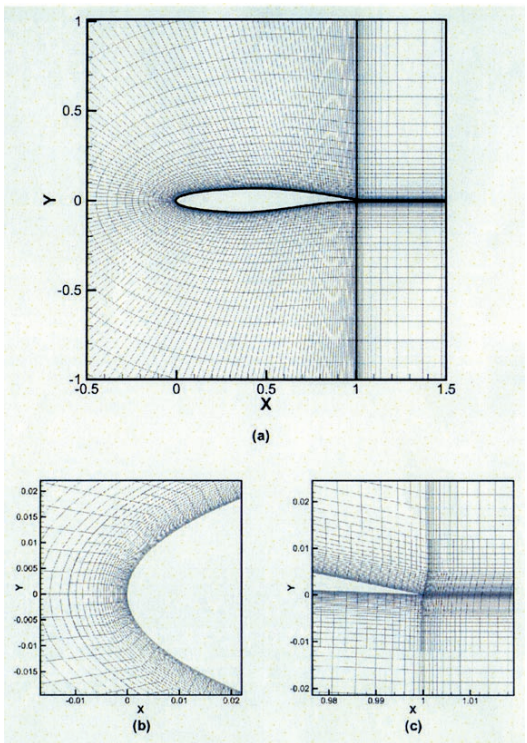

Figure 4. Multi-block grid system for RAE2822 airfoil

Figure 4 shows the two-block grid system with Zonal boundary between fine and coarse grid for RAE2822 airfoil. Near the surface, the density of grid was doubled to get a more accurate solution. Figure 5 shows that the pressure contours are connected smoothly along the Zonal boundary, and C_p curves, as shown in figure 6, show that this refined grid can be used to get as good solutions as fine grid. The pressure coefficient curve shows that calculation result matches well with Cook's experimental data[4], and when using more grids, the results are shown to become better.

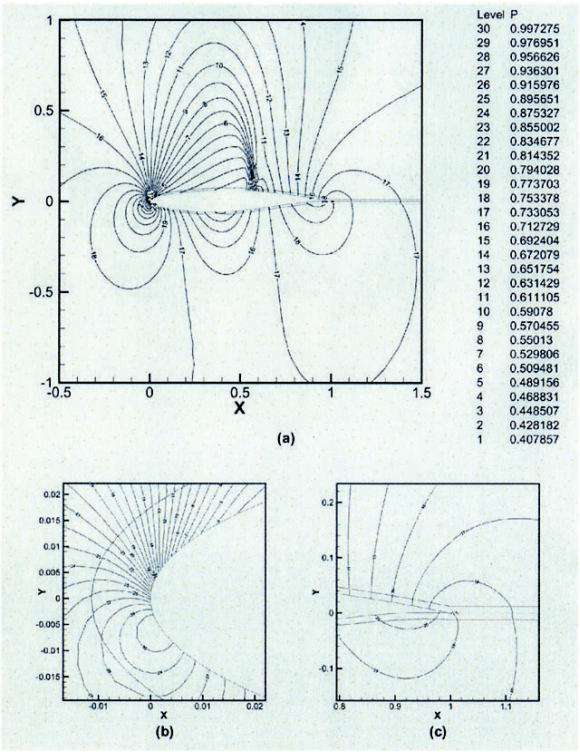

Figure 5. Pressure contours
(M=0.73, Re=6.5x10^6, α =2.79 °, RAE2822 airfoil)

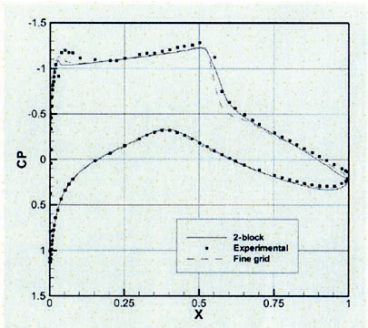

Figure 6. Pressure coefficients along the airfoil surface
(M=0.73, Re=6.5x10^6, α =2.79 °, RAE2822 airfoil)

Flowfields around a NACA0012 airfoil with pitching and/or plunging motions were analyzed by solving two-dimensional unsteady compressible Navier-Stokes equations. An unsteady flowfield of the oscillatory airfoil was given to be the followings: free stream Mach number, M=0.755, Reynolds number in inflow, Re=5.5x10^6. The oscillatory angle of attach is α =0.016 ° +2.51 ° x sin(2Mkt) with the reduced frequency of oscillation, k, which is defined as,

$$k = \frac{\omega c}{2U} = 0.0814$$

where c is the chord length, ω is the angular velocity of oscillation, and U is the inflow velocity.

Figure 7 shows pressure contours at various angles of attack in pitching motion, and figure 8 shows typical unsteady hysteresis of the lift and pitching moment coefficients around oscillating airfoil, which was compared with experimental data[5] .

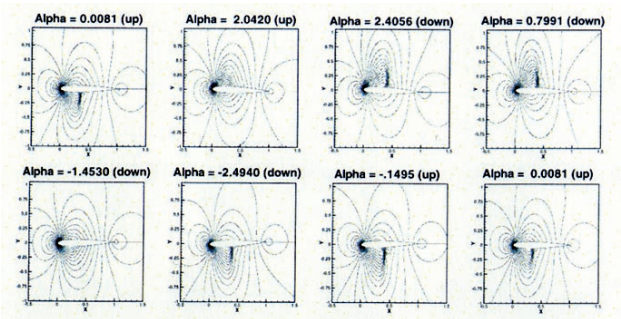

Figure 7. Pressure contours at various angles of attack
(M=0.755,α=0.016°+2.51°xsin(2Mkt),k=0.0814,Re=5.5x10^6)

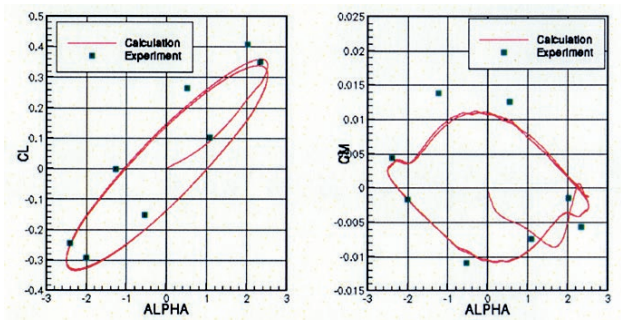

Figure 8. Hysteresis of lift and pitching moment coefficients around a pitching airfoil
(M=0.755,α=0.016°+2.51°xsin(2Mkt),k=0.0814, Re=5.5x10^6)

3.2 Pitching/plunging airfoil

Plunging motion was solved with the vertical displacement analogous to pitching motion. The mean angle of attack was given to be 10 °, and the maximum effective angle of attack by plunging motion can be calculated from equation of the plunging motion by

$$\tan(a_m) = \left(\frac{\dot{h}}{U}\right)_{\max},$$

$$h = h_m \times \cos(\omega t), \quad \dot{h} = -h_m \omega \sin(\omega t),$$

$$h_m = \frac{U}{\omega} \tan a_m$$

where a_m is the magnitude of pitching oscillation, h_m is the magnitude of plunging motion, and $\dot{h}$ is the first derivative of h. The angular velocity of oscillation, ω, was set to be identical with that of pitching oscillation. With above relation, h_m can be expressed with reduced frequency of oscillation, k, after non-dimensionalization,

$$h_m = \frac{1}{2k} \tan a_m$$

In this case, h_m was set in order to make $a_m = 10$ °.

Figure 9 shows the hysteresis of the normal force coefficients and pitching moment coefficients as the amplitude of vertical displacement varies. Like the results of pitching airfoil, lift coefficients shows typical unsteady hysteresis. Lift coefficients become lower during angle of attack increase (nose-up) on account of decrease of effective angle of attack, and become larger during angle of attack decrease (nose-down) on account of increase of effective angle of attack. Navier-Stokes solver makes higher amplitude of oscillation in hysteresis of lift coefficients, which means viscous effect makes higher unsteadiness in plunging motion.

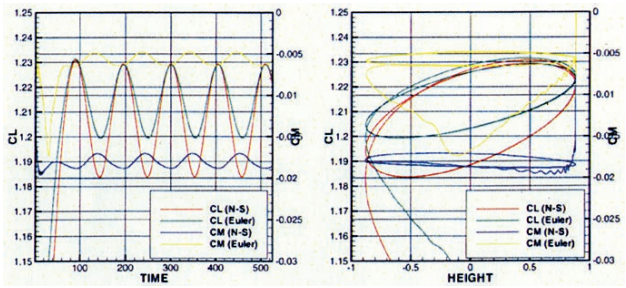

Figure 9. Hysteresis for plunging cases
(M=0.3,α= 10 °, $h_m = 1/2k \tan 10^o$,k=0.1, Re=4.6x10^6)

Next, combined pitching and plunging motion was solved to show wake characteristics of the 2 different types of oscillating motion of the airfoil. Figure 10 shows the hysteresis of the lift force coefficients and pitching moment coefficients as angle of attack and vertical displacement vary including the comparison with those of the case of pitching motion only. Compared with case of pitching motion only, the plunging motion played a role to reduce an unsteadiness of the oscillatory airfoil in this case.

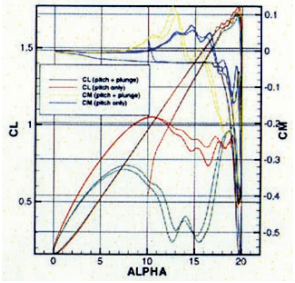

Figure 10. Hysteresis for combined pitching and plunging
(M=0.3, α=10°+10°xsin(2Mkt), k=0.1, Re=4.6x10^6,
$h_m = 1/2k \tan 10^o$)

3.3 2D BWI Model

In the second part, flow interaction between wake and airfoil was solved with two-dimensional compressible unsteady Navier-Stokes solver. Figure 11 shows diagram of interaction between shed vortex and following airfoil. The shed vortex induced from the oscillating airfoil was applied as inflow condition of the following airfoil using periodic boundary condition, which is the simplified two-dimensional model of helicopter rotor blade at the mid-span section.

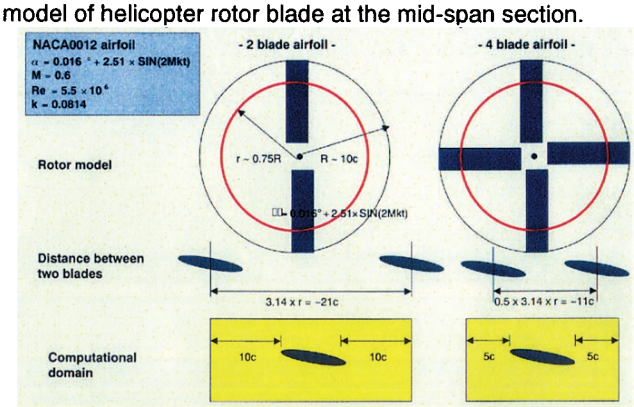

Figure 11. Diagram of interaction between vortex and airfoil

First, successive three NACA0012 airfoils was composed to make one whole computational domain as shown in figure 12. Free stream inflow condition was given to the first airfoil and normal exit condition was applied to the third airfoil. Then for comparison, one airfoil was used to solve the periodic boundary cases. The exit flow was given to the inflow condition repeatedly to simulate periodic boundary condition. For the actual rotor, the movement of two airfoil will be differed according to the azimuth angle, but in this calculation, airfoils were simplified to be synchronized to have the same oscillation movement.

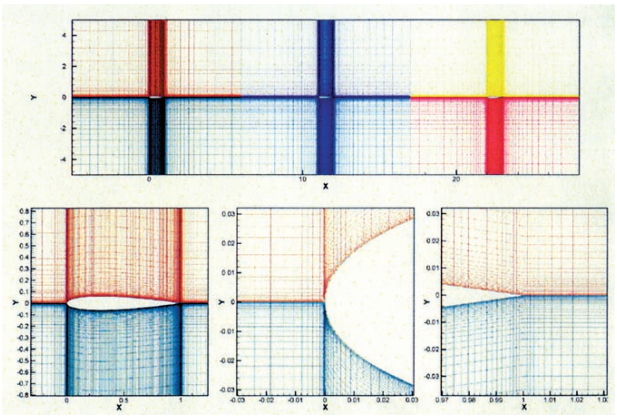

Figure 12. Grid system of successive NACA0012 airfoils

The flow conditions are set to be Mach number equal to 0.6, Reynolds number equal to 5.5x10^6, the oscillatory angle of attack in pitching motion, α, equal to 0.016° +2.51° x sin(2Mkt). The reduced frequency was set to be equal with experiment, k=0.0814.

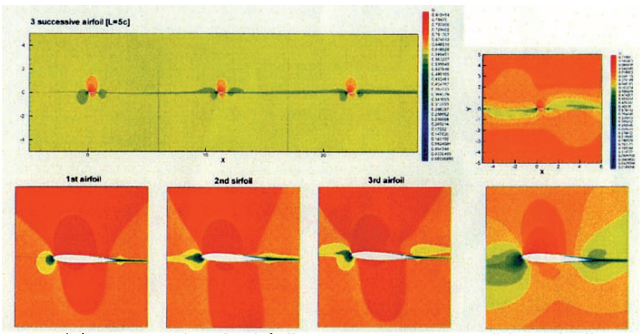

(a) successive 3 airfoils (b) periodic

Figure 13. U-velocity contours
(M=0.755,α=0.016°+2.51° xsin(2Mkt),k=0.0814, Re=5.5x10^6)

Figure 13 shows u-velocity contours for successive 3 airfoils and airfoil with periodic case. The disturbed effects by wake interaction were shown in the 2nd airfoil, the 3rd airfoil, and the periodic case shows much stronger effect.

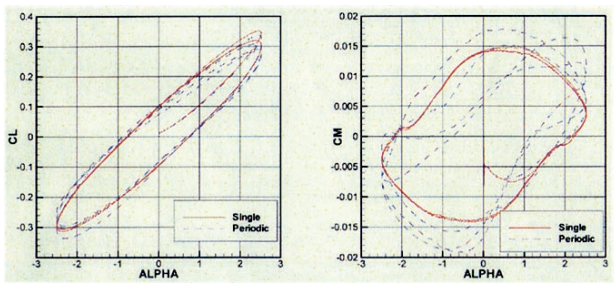

Figure 14. Hysteresis of lift and pitching moment coefficients around a pitching airfoil for single and periodic conditions
(M=0.755,α=0.016°+2.51° xsin(2Mkt),k=0.0814, Re=5.5x10^6)

Figure 14 shows the comparison of the hysteresis of lift and pitching moment coefficients around a pitching airfoil for single airfoil with normal flow field condition (single) and periodic boundary condition. In the case using periodic boundary condition, the wake which was caused by the former blade altered the following airfoil. The induced wake

of the pitching airfoil, which was effected by the following airfoil, with various grid systems was used to show that grid refinement method can be available in reducing the numerical dissipation.

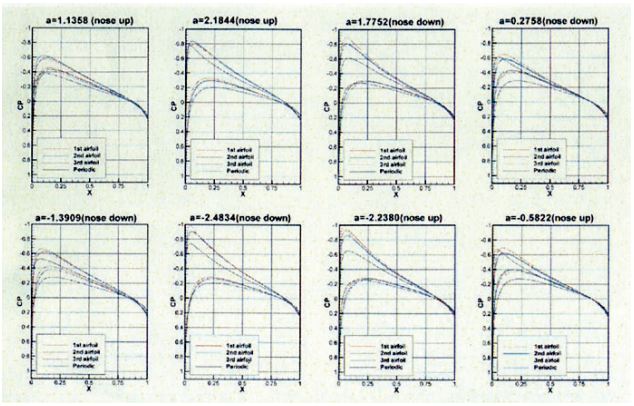

(a) L=5c

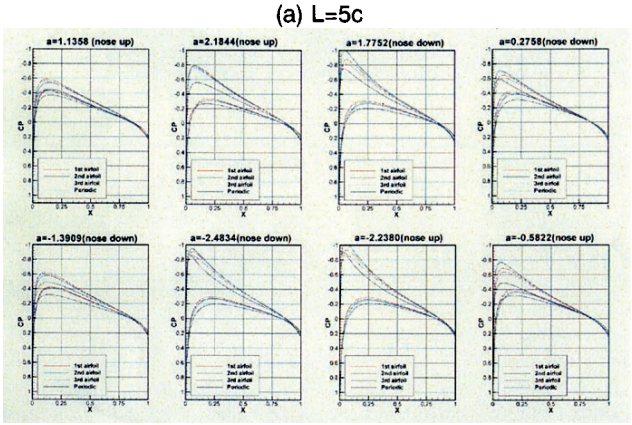

(b) L=10c

Figure 15. Comparison of pressure coefficients for 3 airfoil and periodic airfoil at various angles (M=0.755,α=0.016°+2.51° xsin(2Mkt),k=0.0814, Re=5.5x10^6)

Figure 15 shows comparison of pressure coefficients for 3 airfoil and periodic airfoil at various angles. The whole tendency of pressure coefficients is similar, but as interaction goes on (starting from first airfoil with no interaction to periodic airfoil with enough interaction), the peak point of pressure coefficient decreases.

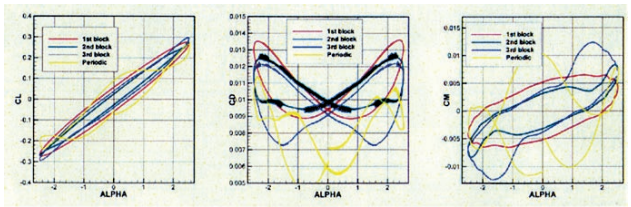

(a) L=5c

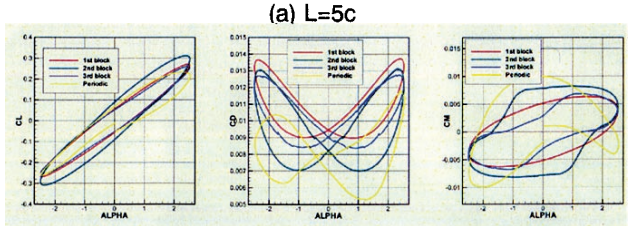

(b) L=10c

Figure 16. Unsteady hysteresis of lift, drag and pitching moment coefficients around a pitching airfoil (M=0.755,α=0.016°+2.51° xsin(2Mkt),k=0.0814, Re=5.5x10^6)

Figure 16 shows unsteady hysteresis of lift, drag and pitching moment coefficients for successive three airfoils for 2 blade (L=10c) and 4 blade (L=5c) and periodic case. Interaction with wake affects on maximum/minimum angles of attack, then the hysteresis were altered to be irregular, and finally became quite different for periodic case. Considering the length of the wake region, the case with 5 chord length shows to be much affected by interaction and makes more disturbed shapes. Figure 17 shows time history of pressure value at 2 points above/below the trailing edge for the case of successive 3 airfoils and case of periodic boundary condition. Sampling points are located upper and lower points very near the surface and trailing edge. Compared with the fact that 1st airfoil has quite simple sinusoidal wave form, the 2nd and the 3rd airfoils show more disturbed wave form, and the case of periodic boundary condition shows much complicated waves with higher frequencies.

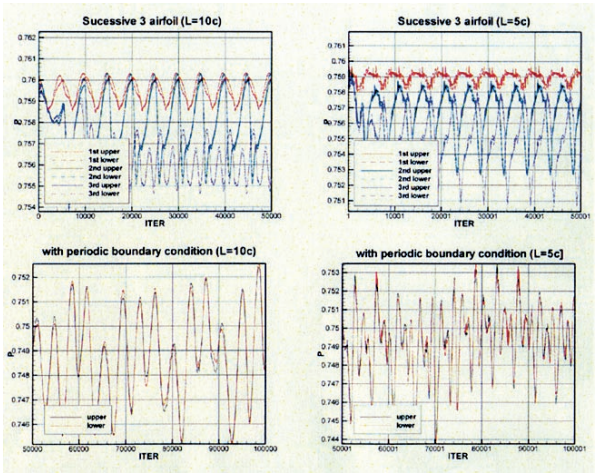

Figure 17. Time history of pressure near trailing edge points (M=0.755,α=0.016°+2.51° xsin(2Mkt),k=0.0814, Re=5.5x10^6)

By doing Fast Fourier Transform (FFT) analysis, these higher frequencies can be seen in spectrums. Figure 18 shows FFT results for same pressure histories at upper point. As shown here, compared with basic frequency of airfoil oscillating in sinusoidal wave, twice and three times higher frequencies appear, and these higher frequencies become stronger as interaction repeats itself. The case of periodic boundary condition shows that higher frequencies become more dominant. Figures 18 (a) and (b) show FFT analysis for lift coefficient for L=5c, 10c. As flows encounter the interaction from first airfoil, the higher frequency characteristics occur, and the effects become stronger in the periodic conditions and in the case of L=5c. Figures 18 (c) to (f) show drag and pitching moment coefficients for L=5c, 10c. Figures 18 (g) and (h) are the FFT results for pressure at one point near trailing edge.

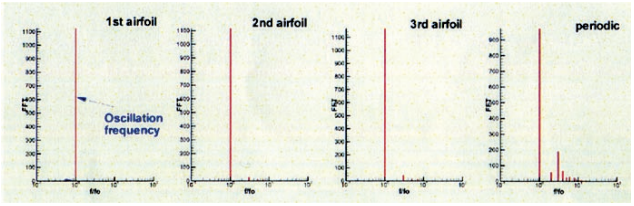

(a) Lift coefficient for L=5c

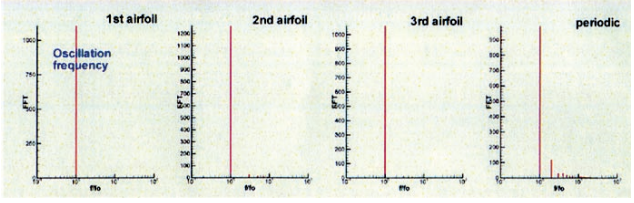

(b) Lift coefficient for L=10c

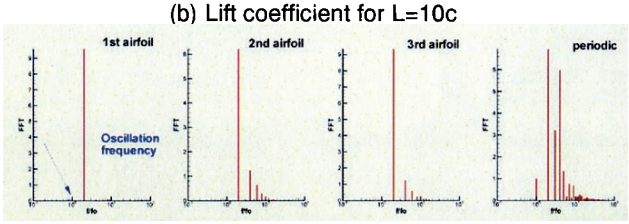

(c) Drag coefficient for L=5c

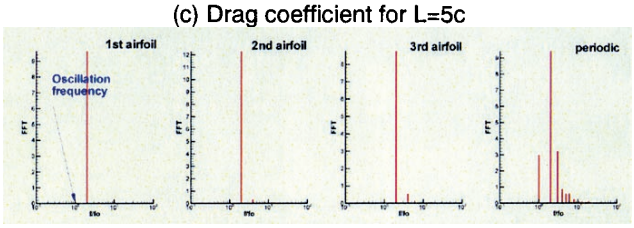

(d) Drag coefficient for L=10c

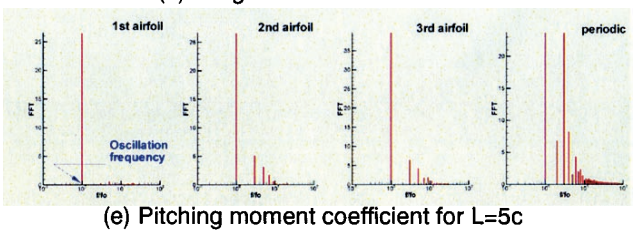

(e) Pitching moment coefficient for L=5c

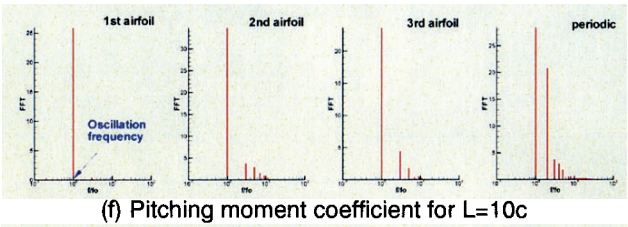

(f) Pitching moment coefficient for L=10c

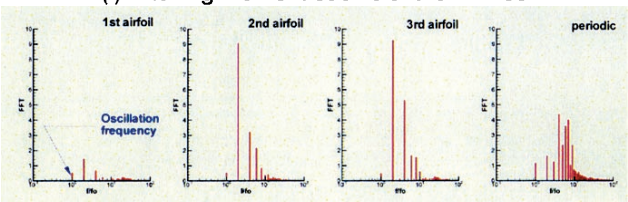

(g) Pressure at a point near trailing edge for L=5c

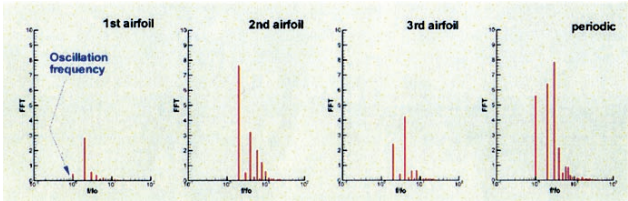

(h) Pressure at a point near trailing edge for L=10c

Figure 18. Hysteresis of lift and pitching moment coefficients around a pitching airfoil for single and periodic condition (M=0.755,α=0.016°+2.51° xsin(2$M$$k$$t$),$k$=0.0814, Re=5.5x10^6)

4. Conclusions

As a step to develop the solution technique for the flowfield around a helicopter rotor blade, two-dimensional, steady Navier-Stokes equation were solved using grid-refined multi-block system in parallel computing. Flow analysis of RAE2822 airfoil shows effectiveness of this method in computation cost with equal accuracy by comparing several aerodynamic coefficients with experimental data.

Flowfields around a NACA0012 airfoil in pitching and plunging motion were analyzed by solving two-dimensional compressible Navier-Stokes equations. In analysis of the oscillatory pitching airfoil, the unsteady characteristics such as hysteresis of aerodynamic coefficients can be successfully simulated. Grid clustering in wall region was found to have a quite large effect on the numerical accuracy. In the analysis of plunging motion, a similar unsteady hysteresis of aerodynamic coefficients was shown, which caused by the variation of the effective angle of attack. The flow solution of the combined pitching and plunging motion shows the effect of 2 different types of oscillating motion of the airfoil, where plunging effect on aerodynamic characteristics is comparably small but worthy to be considered.

Blade-Wake Interaction (BWI) was simulated with simple 2D model to show the effect of wake interaction with the following airfoils. Three successive airfoils and an airfoil with periodic condition were used to show that as interaction goes on, higher frequency in flow characteristics was produced and became stronger.

With the above research, we can conclude the followings.

(1) grid refinement method is effective in reducing the numerical dissipation using relatively small computing power.
(2) the interaction with the blade and its wake produced high-frequency fluctuation and wake itself was highly disturbed.
(3) three successive airfoils, even they show the effect of wake interaction, is not enough to get periodic solution as those in helicopter rotor. It means that undisturbed vortex (wake) is insufficient to account for BWI analysis and that wake interaction should be well-considered in helicopter rotor noise problem.

To increase the efficiency of computation, research on the domain decomposition and Zonal boundary should be carried out together with research on parallel computation.

5. Acknowledgement

The authors would like to thanks to Dr. Shigeru Saito and many members in National Aerospace Laboratory (NAL) for their assistance and advice.

This work has been supported by the Japan International Science and Technology Exchanging Center (JISTEC).

6. References

[1] Brook, T. F., Jolly, J. R., Marcolini, M. A. (1988) *Helicopter main-rotor noise*, NASA Technical Paper 2825

[2] Roe, P. L. (1981) *Approximate Riemann solvers, parameter vectors, and differenece schemes.* Journal of Computational Physics, Vol.43:357-372.

[3] Bram van Leer (1982) *Flux-Vector Splitting For The Euler Equations*, Lecture Notes on Physics, Vol. 170, pp. 507-512

[4] Cook, P., McDonald, M. and Firmin, M., (1979) *Aerofoil RAE2822 - pressure distribution and boundary layer wake measurements*, AGARD R-138

[5] Landon, R.H., (1982) *NACA0012 oscillatory and transient pitching*, AGARD R-702